

1 **RADIATIVE FORCING BY CO₂ OBSERVED AT**
2 **TOP OF ATMOSPHERE FROM 2002-2019**

3 **C. P. Rentsch**

4 Midland, MI, USA

5 **Key Points:**

- 6 • The Atmospheric Infrared Sounder (AIRS) offers the longest observational record
7 among all current and previous satellite spectrophotometers.
8 • Seventeen years of global nighttime, cloud-clear spectral radiance measurements
9 reveal $0.358 \pm 0.067 \text{ Wm}^{-2}$ of CO₂-induced radiative forcing.
10 • Observed CO₂ forcing is 70% of the effective radiative forcing predicted by the IPCC
11 5th Assessment Report.

Abstract

Spectroscopic measurements at top-of-atmosphere are uniquely capable of attributing changes in Earth's outgoing infrared radiation field to specific greenhouse gasses. The Atmospheric Infrared Sounder (AIRS) placed in orbit in 2002 has spectroscopically resolved a portion of Earth's outgoing longwave radiation for 17 years. Concurrently, atmospheric CO₂ rose from 373 to 410 ppm, or 28% of the total increase over pre-industrial levels. The IPCC Fifth Assessment Report predicted $0.508 \pm 0.102 \text{ Wm}^{-2}$ additional radiative forcing from this CO₂ increase. Here it is shown that global measurements under nighttime, cloud-clear conditions reveal $0.358 \pm 0.067 \text{ Wm}^{-2}$ of CO₂-induced radiative forcing, or 70% of IPCC model predictions.

Introduction

Increasing infrared absorption caused by rising CO₂ is the foundational physical mechanism underpinning the anthropogenic global warming hypothesis. Despite numerous studies on global temperature trends and rising greenhouse gas concentrations, very few investigations offer long term spectrophotometric measurement of CO₂ altering Earth's outgoing longwave radiation (OLR). Harries et al. (2001) compared 529 OLR spectra measured by the IRIS satellite in 1970 to 4,061 spectra measured by IMG in 1996 over the Pacific Ocean. Feldman et al. (2015) reported increasing downwelling longwave radiation (DLR) in two 1.6° conical upward views of the atmosphere between 2000 and 2010 (figure 1). Neither study provides a global assessment of CO₂-induced radiative forc-

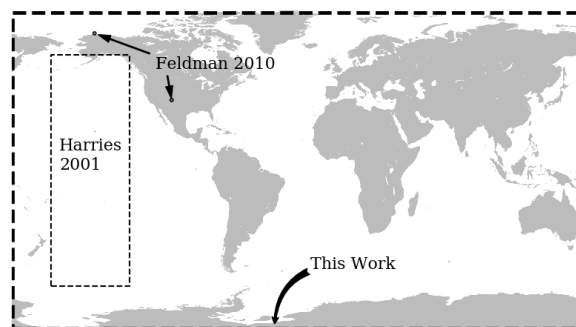


Figure 1. Measurement coverage for this work and select prior works by others

ing. The Atmospheric Infrared Spectrophotometer (AIRS) offers the longest record among all current or previous satellite spectrophotometers and has measured Earth's OLR while atmospheric CO₂ concentration rose from 373 to 410 ppm, 28% of the total increase since 1750. This work examines 50.7 billion global nighttime, cloud-clear spectral radiance measurements (hereafter: radiances) made by AIRS during the last seventeen years. Figure 2 exemplifies a single OLR spectrum comprised of 2,378 radiances. AIRS does not have measurement capability at $<649.6 \text{ cm}^{-1}$, $1136\text{-}1217 \text{ cm}^{-1}$ or $1614\text{-}2181 \text{ cm}^{-1}$.

1 Data

The majority of satellite views of Earth contain clouds that reflect or absorb upwelling infrared (IR). Cloud-clear scenes are preferred to avoid attributing cloud-induced OLR reductions to CO₂. The AIRS version 6 level 2 data product (Teixeira, 2013) quantifies fractional cloud content (*Tot_Cld4_CCfinal* field in *AIRS2CCF.006*) ranging from 0.00 to 1.00. This work utilizes radiances with 0.00 cloud fraction; only 11% or radiances

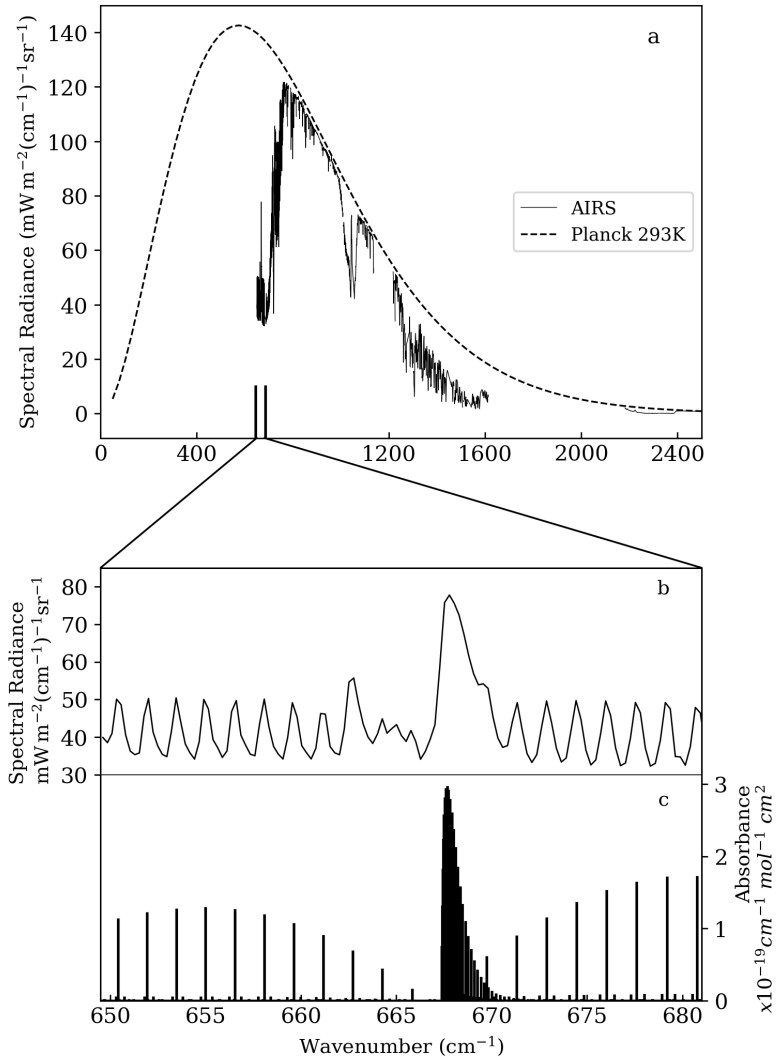


Figure 2. [a] AIRS nighttime, cloud-clear OLR spectrum and 293K Planck distribution, [b] 650-680 cm^{-1} subset, [c] HITRAN2016 spectral absorbance lines for CO_2 (Gordon et al., 2017). Note the excellent coincidence between AIRS detected radiance peaks and HITRAN CO_2 absorbance lines.

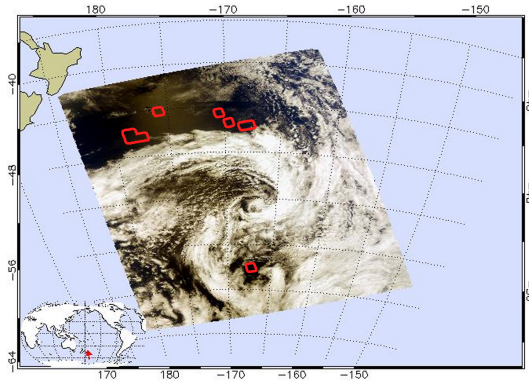


Figure 3. Visible image from granule 015 collected on January 1, 2016. Cloud-clear regions identified by the algorithm outlined in red.

45 meet this criterion. Although AIRS Level 2 measurements are a cloud-cleared data prod-
 46 uct, only naturally cloud-clear radiances with no mathematical adjustments contribute
 47 to this analysis. Figure 3 provides a cloud-clear selection example rendered from the sun-
 48 lit side of Earth to permit comparison with a visible image, however no daytime OLR
 49 measurements contributed to this analysis. It is evident that the cloud detection algo-
 50 rithm is conservative: visibly cloud-clear areas were not included and no visibly cloud-
 51 contaminated areas were inadvertently included (in this example the cloud detection al-
 52 gorithm has false positives but no false negatives).

53 Solar longwave infrared radiation reflected by clouds or Earth’s surface will com-
 54 bine with terrestrial OLR, contaminating daytime measurements. To eliminate this source
 55 of error, only nighttime measurements were utilized. When the AIRS solar zenith an-
 56 gle (SZA) is $<90^\circ$ AIRS observes the sunlit side of Earth, when $90^\circ < \text{SZA} < 108^\circ$ it ob-
 57 serves the twilight region and when $\text{SZA} \geq 108^\circ$ it observes the nighttime region. Only
 58 measurements at $\text{SZA} \geq 108^\circ$ were utilized.

59 The AIRS mirror scans $\pm 49.5^\circ$ from nadir and higher scan angles observe IR emis-
 60 sion from higher in the atmosphere. Radiances from scan swath edges are signif-
 61 icantly warmer or colder than nadir observations in the bands of radiatively-active gasses.
 62 To reduce the effects of this anisotropy, only radiances at scan angles $\leq 25^\circ$ were utilized.

63 The 2,378 individual channels comprising the AIRS IR sensor are monitored for
 64 quality and flags are raised (0-2) whenever any should degrade. Measurements with qual-
 65 ity value 0 “highest quality” and 1 “useful for scientific measurement” were utilized, while
 66 quality value 2 “do not use” were excluded. Radiance measurements flagged as dust-contaminated
 67 were similarly excluded, though these were rare ($<0.01\%$).

68 2 Method

69 All AIRS radiance measurements meeting the selection criteria were analyzed in
 70 this study (not a subset). Radiances for a given wavenumber channel were binned by month,
 71 sub-binned in 10° latitude increments, then averaged. For example, 4,554 nighttime, cloud-
 72 clear radiances at 650.814 cm^{-1} measured between 0° and 10°N contribute to the aver-
 73 age radiance for January 2013 (figure 4, inset). 28.8% of sub-bins contain no data due
 74 to heavy clouds, lack of nighttime measurements (e.g., polar summers) or failed detec-
 75 tor channels. An additional 1.2% of all sub-bins containing fewer than 25 radiances meet-
 76 ing the selection criteria were excluded to prevent trend skew by only a few measurements.
 77 The median number of radiance measurements contributing to a monthly average for a

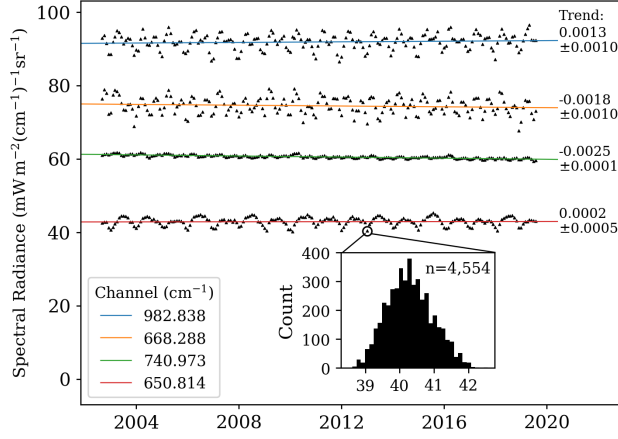


Figure 4. Least-squares regression fit to average monthly radiances for four AIRS channels in 0° - 10° latitude bin. Remaining channels in all latitude bins were fit similarly.

78 given channel in a given latitude bin is 5,064. Over time, some channel detectors suc-
 79 cumb to solar radiation exposure and cease useful data production. Of the maximum
 80 potential 17 year record, channels with fewer than five years were excluded for insuffi-
 81 cient record length.

82 A straight line was fit by least-squares regression to the time series of monthly ra-
 83 diance averages for each channel in each latitude bin. Seasonal temperature cycling was
 84 eliminated as a source of trend bias by utilizing only complete years of measurement data
 85 starting on 1 September 2002 and ending on 31 August 2019. An example line fitting
 86 is provided in figure 4. The slope of each line is the spectral radiance trend $\dot{L}_{\tilde{\nu}}$ ($\text{mW m}^{-2}(\text{cm}^{-1})^{-1}\text{sr}^{-1}\text{yr}^{-1}$)
 87 and the uncertainty is $\pm 1\sigma$. Lines were fit to all channels in all 18 latitude bins.

88 3 Results: CO₂ Radiative Forcing

89 Reductions in OLR at 650-756 cm^{-1} are presumed the result of rising atmospheric
 90 CO₂ concentration. The reductions at detectable portions of the CO₂ P, Q, and R-branches
 91 (650-682 cm^{-1}) are minor compared to 687-756 cm^{-1} where the majority of detectable
 92 OLR reduction coincides with one of the CO₂ wings. OLR flux density change δE (Wm^{-2})
 93 was produced by integrating the spectral radiance trend $\dot{L}_{\tilde{\nu}}$ over the range of CO₂-affected
 94 wavenumbers, then multiplying by 17 years and by π sr, regarding the atmosphere as a
 95 Lambertian emitter at these optically-thick channels:

$$96 \quad \delta E_{PQR} = 17\pi \int_{649.6\text{cm}^{-1}}^{682.0\text{cm}^{-1}} \dot{L}_{\tilde{\nu}} d\tilde{\nu} = -0.031 \pm 0.014 \text{ Wm}^{-2} \quad (1)$$

$$97 \quad \delta E_{wing} = 17\pi \int_{687.6\text{cm}^{-1}}^{756.3\text{cm}^{-1}} \dot{L}_{\tilde{\nu}} d\tilde{\nu} = -0.164 \pm 0.033 \text{ Wm}^{-2} \quad (2)$$

99 Integrals are depicted in the figure 6 inset, shaded regions. The majority of detectable
 100 flux density change is attributable to the increasing wing absorption at 687-756 cm^{-1} .
 101 The symmetrical wing at 580-650 cm^{-1} is outside of AIRS measurement range (see fig-
 102 ure 7). Consequently, (1) + (2) is only a partial measurement of δE caused by rising
 103 CO₂ and δE_{total} must be estimated. The P-branch and R-branch absorption lines flank-
 104 ing the Q-branch are nearly symmetrical and rising CO₂ caused nearly-identical reduc-
 105 tions in radiance. By extension, it is a reasonable prediction that the unmeasured 580-
 106 650 cm^{-1} wing has undergone OLR reduction by an amount similar to the measured 687-

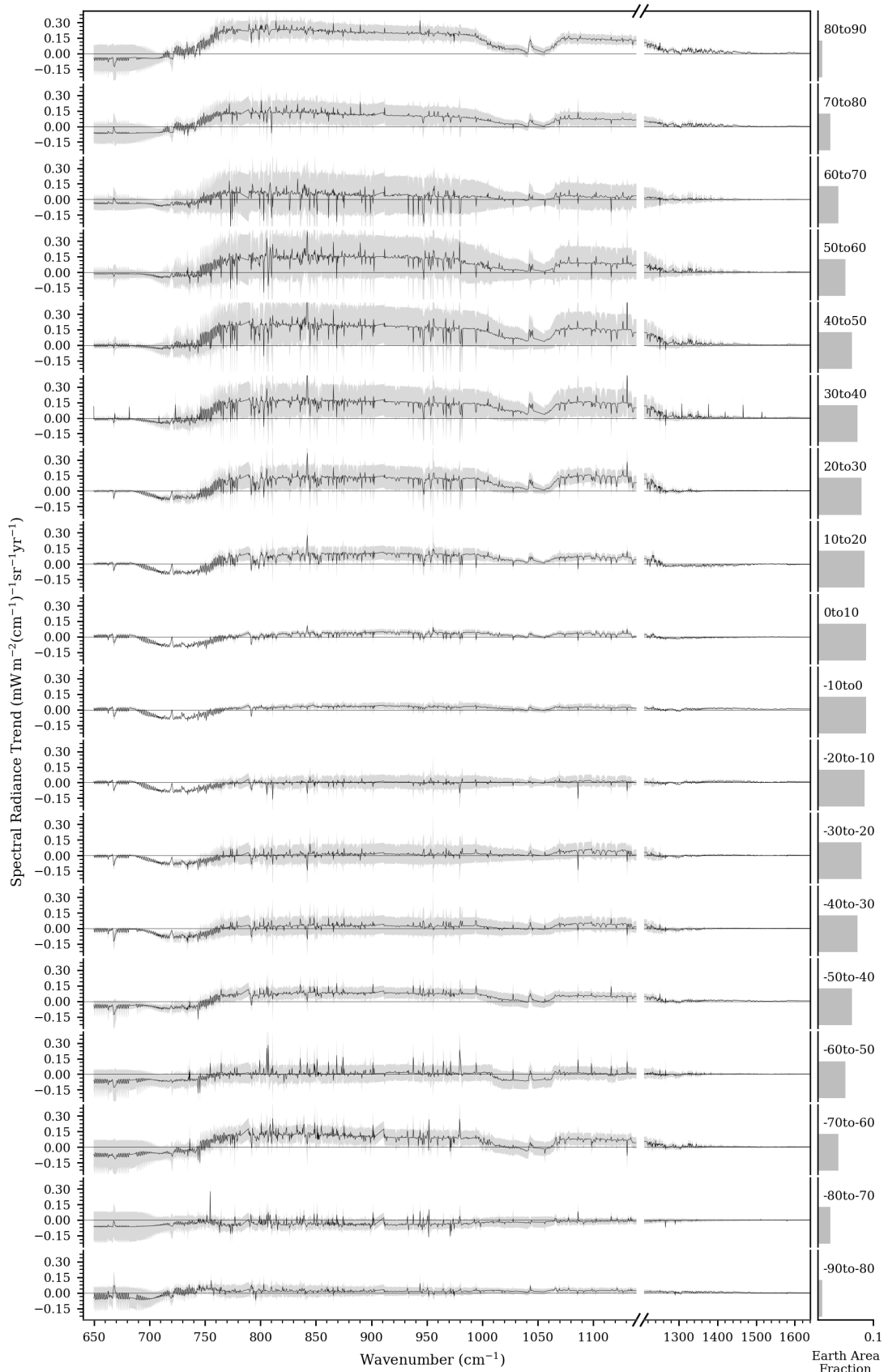


Figure 5. Nighttime, cloud-clear spectral radiance trend 2002-2019 in 10° latitude increments. $\pm 1\sigma$ shaded.

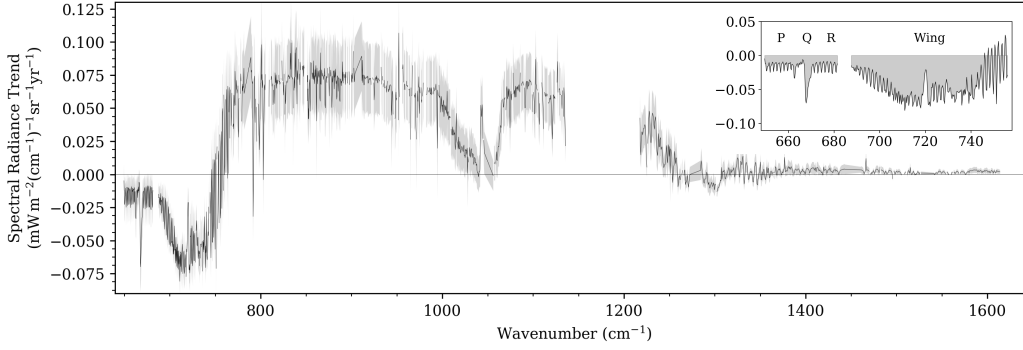


Figure 6. Global composite nighttime, cloud-clear spectral radiance trend 2002-2019. $\pm 1\sigma$ shaded. Inset illustrates the integrals assessed to determine OLR reduction attributable to rising CO_2 .

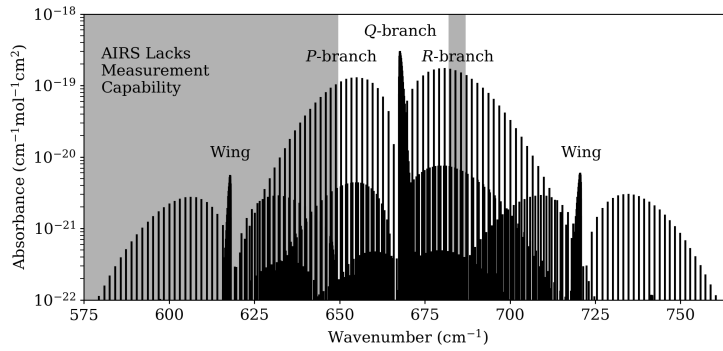


Figure 7. HITRAN2016 CO_2 v_2 absorption lines and AIRS measurement ranges

107 756 cm^{-1} wing. Therefore, total OLR flux density reduction due to rising CO_2 is esti-
 108 mated as:

$$109 \quad \delta E_{total} = \delta E_{PQR} + 2\delta E_{wing} = -0.358 \pm 0.067 \text{ W m}^{-2} \quad (3)$$

110 The computed flux density change, with reversed sign, is termed *radiative forcing* (RF).
 111 It is reasonable to view (1) + (2) as a partial global measurement of nighttime, cloud-
 112 clear CO_2 RF and (3) as an empirically-derived estimation of total nighttime, cloud-clear
 113 CO_2 RF added between 2002-2019.

114 Measurement of the atmospheric CO_2 concentration increase that produced this
 115 additional forcing was supplied by the NOAA ESRL's global monitoring division (Dlugokencky
 116 & Tans, 2019). The combination of empirical measurement of TOA RF and CO_2 con-
 117 centration change permits a direct comparison to the climate model predictions of CO_2 -
 118 induced effective radiative forcing (ERF) taken from the IPCC's Fifth Assessment Re-
 119 port (Stocker et al., 2013), also known as AR5. ERFs for 2000-2020 (368.9-412.1 ppm
 120 CO_2) were interpolated for 2002-2019 (373.1-410.5 ppm CO_2) and compared to AIRS
 121 measurements in table 1.

122 AR5 ERFs were computed while holding surface temperature constant, a condi-
 123 tion that does not hold for Earth. Therefore, an additional comparison was sought to
 124 AIRS measurements of locations where surface/lower tropospheric temperatures did not
 125 significantly change. Window wavenumber trends in Figure 5 indicate this is largely true
 126 for 10°N - 40°S and the area-weighted average forcing for this latitude range was included
 127 in table 1. In either case, AR5 climate models appear to over-predict CO_2 RF.

Table 1. Radiative Forcing from +37 ppm CO₂

Source	$-\delta E_{total} \pm 1\sigma$ (Wm ⁻²)
AIRS 90°N-90°S	0.358±0.067
AIRS 10°N-40°S	0.434±0.047
IPCC AR5 ERF	0.508±0.102

128 4 Sources of Error

129 Radiance and flux density changes in the CO₂ *v*₃ band (2300-2380 cm⁻¹) were not
 130 characterized since less than 0.01% of the Earth's infrared radiant exitance occurs in this
 131 band.

132 The AIRS instrument measurement gap at 681.993-687.601 cm⁻¹ prevents trend
 133 quantification in a narrow portion of the *v*₂ R-branch. Interpolation from adjacent chan-
 134 nels yields 0.0038 Wm⁻² of forcing was not measured, causing underestimate of δE_{total}
 135 by 1.2%.

136 The unmeasured 580-650 cm⁻¹ wing was assumed to undergo radiance reduction
 137 identical to the measured wing, however, the 580-650 cm⁻¹ wing overlaps with stronger
 138 water vapor absorption lines. The assumption of symmetry is conservatively high and
 139 actual OLR reductions at 580-650 cm⁻¹ are expected to be lower than at 687-756 cm⁻¹.
 140 Trend asymmetry between the two wings was observed in DLR reported by Feldman et
 141 al. (2015): the 580-650 cm⁻¹ wing showed less forcing change over time relative to the
 142 687-756 cm⁻¹ wing, particularly in the southern great plains where atmospheric mois-
 143 ture content is higher.

144 Over 17 years, detector stability is more important than absolute accuracy as un-
 145 biased noise does not preclude long-term trend analysis. One possible cause of trend bias
 146 is gradual accumulation of molecular contaminants on the AIRS detector mirror. A hy-
 147 pothetical 100Å contamination layer is predicted by H. Aumann et al. (2000) to increase
 148 the mirror emissivity variation by 0.001, producing cold scene brightness temperatures
 149 at 650-800 cm⁻¹ that are 0.1-0.2° K warmer than reality. If such a contamination layer
 150 were gradually building up during the observation period, warming trends could be am-
 151 plified and cooling trends (including forcing) could be diminished. Evidence of mirror
 152 contamination between 2002-2010 has been reported by others (H. H. Aumann et al.,
 153 2018) to affect AIRS midwave IR channels (2181-2665 cm⁻¹) which were not utilized in
 154 this study.

155 This analysis assumed isotropic atmospheric emissions despite radiances from scan
 156 swath edges measuring significantly warmer or colder than nadir observations. Over time,
 157 if proportionally more (or fewer) swath edge measurements meet the quality and cloud-
 158 clear selection criteria, trend bias will result. As a check, trend fits and integrals were
 159 recomputed with a wider and narrower scan angle ranges, including and excluding larger
 160 portions of scan swath edges. Fewer total measurements contribute to a restricted scan
 161 angle analysis with a commensurate increase in uncertainty. Results in table 2 indicate
 162 that including scan swath edges causes overestimation of forcing: δE_{total} produced from
 163 $\pm 25^\circ$ and $\pm 49.5^\circ$ measurements are 3.8% and 10.4% higher than from $\pm 12.5^\circ$ measure-
 164 ments, respectively.

Table 2. Swath Edge Radiance Impact

Scan Angle	Radiances at 650-756 cm^{-1} (count)	CO_2 Forcing $-\delta E_{total} \pm 1\sigma (\text{Wm}^{-2})$
$\pm 49.5^\circ$	25.7×10^9	0.381 ± 0.067
$\pm 25.0^\circ$	15.5×10^9	0.358 ± 0.067
$\pm 12.5^\circ$	7.8×10^9	0.345 ± 0.068

5 Conclusion

Seventeen years of AIRS nighttime, cloud-clear OLR measurements reveal $0.358 \pm 0.067 \text{ Wm}^{-2}$ additional radiative forcing induced by +37 ppm atmospheric CO_2 . Unfortunately, AIRS lacks measurement capability at 580-650 cm^{-1} for complete CO_2 ν_2 band characterization, therefore this empirical estimate of increased forcing was devised by presuming CO_2 ν_2 wing symmetry and doubling the observed wing's radiative forcing. The IPCC Fifth Assessment Report predicted $0.508 \pm 0.102 \text{ Wm}^{-2}$ RF resulting from this CO_2 increase, 42% more forcing than actually observed. The lack of quantitative long-term global OLR studies may be permitting inaccuracies to persist in general circulation model forecasts of the effects of rising CO_2 or other greenhouse gasses.

Acknowledgments

The author acknowledges Robert Amour and Leon de Almeida for analysis program creation, Nolan Nicholson for the custom data plotting program and Steven J. Martin for the many informative conversations. All code for analysis replication is available at <https://github.com/rentcp/Heatwave>.

References

- Aumann, H., Gregorich, D., Gaiser, S., Hagan, D., Pagano, T., Strow, L., & Ting, D. (2000). Airs algorithm theoretical basis document. *Level 1B, Part, 1*, 70.
- Aumann, H. H., Manning, E. M., & Broberg, S. (2018). Radiometric stability in 16 years of airs hyperspectral infrared data. In (Vol. 10764, p. 1076400).
- Dlugokencky, E., & Tans, P. (2019). *Noaa/esrl*. www.esrl.noaa.gov/gmd/ccgg/trends/. (Accessed 11-2019)
- Feldman, D. R., Collins, W. D., Gero, P. J., Torn, M. S., Mlawer, E. J., & Shippert, T. R. (2015). Observational determination of surface radiative forcing by CO_2 from 2000 to 2010. *Nature*, *519*(7543), 339.
- Gordon, I. E., Rothman, L. S., Hill, C., Kochanov, R. V., Tan, Y., Bernath, P. F., ... others (2017). The hitran2016 molecular spectroscopic database. *Journal of Quantitative Spectroscopy and Radiative Transfer*, *203*, 3–69.
- Harries, J. E., Brindley, H. E., Sagoo, P. J., & Bantges, R. J. (2001). Increases in greenhouse forcing inferred from the outgoing longwave radiation spectra of the earth in 1970 and 1997. *Nature*, *410*(6826), 355.
- Stocker, T. F., Qin, D., Plattner, G.-K., Tignor, M., Allen, S. K., Boschung, J., ... others (2013). Climate change 2013: The physical science basis.
- Teixeira, A. S. T. (2013). *Airs/aqua l2 cloud-cleared infrared radiances (airs-only) v006*. <https://doi.org/10.5067/Aqua/AIRS/DATA205>. (Accessed 10-2019)